Monatshefte für Chemie 136, 2007–2016 (2005)
DOI 10.1007/s00706-005-0374-z

Monatshefte für Chemie
Chemical Monthly
Printed in Austria

Sulfated Alumina Catalysts: Consequences of Sulfate Content and Source

Gamal A. H. Mekhemer, Hussein A. Khalaf, Seham A. A. Mansour, and **Ahmed K. H. Nohman***

Chemistry Department, Faculty of Science, Minia University, El-Minia 61519, Egypt

Received January 11, 2005; accepted (revised) April 13, 2005
Published online November 11, 2005

Summary. Consequences of the loading level of sulfate ions (3, 6, and 10-wt%) as well as the source of sulfate (H_2SO_4 or $(NH_4)_2SO_4$) on the structural, textural, and surface acid–base properties as well as the impacts on catalytic activity towards 2-propanol conversions on γ-Al_2O_3 and on aluminum hydroxide gel is described. Structural investigations of the catalysts by XRD revealed that the sulfation processes do not remarkably affect the γ-phase of alumina irrespective of the sulfate content or source. N_2-adsorption at 77 K indicated that sulfated gel catalysts exhibit the highest S_{BET} areas and, in general, S_{BET} for all catalysts were found to decrease with the increase of sulfate content, such a decrease is more pronounced for the 10% loaded catalysts. Pyridine adsorption as followed by FTIR indicated that sulfation of alumina increases the strength of its *Lewis* acid sites and creates *Brønsted* acidity in the case of highly loaded catalysts. The catalytic decomposition of 2-propanol in the gas phase indicated that, amongst all the catalysts investigated, the 6% loaded ones exhibited 100% activity (2-propanol conversion) and the highest propene (dehydration product) selectivity.

Keywords. Alumina; Dehydration; Pyridine; Sulfate; 2-Propanol.

Introduction

Because many catalytic materials can not easily be prepared in the form of small particles or suitably robust high-surface area particles, they may be dispersed as minute particles on a sturdy high-surface area support, *e.g.*, γ-Al_2O_3 [1]. It is one of the transition aluminas most widely applied as catalyst support. This is due to reasons of commercial as well as preparation availability. Furthermore, it is stable at relatively high temperatures, mechanically stable, exposing *Lewis* acid sites, easily formed with high surface area, and in a variety of pore structures [2].

Sulfated metal oxides (particularly sulfated zirconia) have attracted the attention of many researchers in the last few years. This is actually due to their higher activity in reactions for which acid catalysis plays a key role in many important

* Corresponding author. E-mail: nohmana@yahoo.com

catalytic processes in the chemical and petroleum industries. Some metal oxides doped with sulfate give rise to new solid acid catalysts which have high acidity. The doping effect of sulphur on specific surface areas and crystallographic phase transitions are now well established. The use of sulfate as acidity promoting additives for catalytic aluminas has been reported [3] and this effect has been suggested to arise at least partly from changes in acidity, and to be twofold [4]. Sulfates play an important role as support stabilizer [5, 6], the stabilizing effect seems to delay the most undesired phase transition of γ-Al_2O_3. The stability and the surface acidity of sulfated catalysts are indeed directly dependent on the sulfation process as well as on the textural properties of the parent alumina gel [7]. The introduction of a small amount of sulphur compounds onto metal oxides enhanced remarkably the acidic properties of the oxides, regardless of the types of the introduced sulphur compounds, for example $(NH_4)_2SO_4$, H_2S, or H_2SO_4, provided that the optimal calcination temperature is applied and that sulphur species are fully oxidized [8–10]. The structure of the acidic species has been proposed to be a surface complex which is comprised of a metal cation and sulfate ions with two covalent S=O bonds [9]. Transformations of the introduced sulphur compounds to acidic species were also proposed [9, 10]. Most of the previous studies have applied the same catalyst preparation techniques [11, 12]. Namely alumina gel formed by the precipitation with ammonium hydroxide was impregnated with a sulfate source of variable concentrations.

In this work we aimed at exploring the effect of different sulfate loads and sources on: i) the bulk structural and textural characteristics of γ-alumina (*AlO* series) in comparison to aluminium hydroxide (dried gel, *AlH* series), ii) the surface acidity of these catalysts as revealed by FTIR spectra of adsorbed pyridine vapour, and iii) the decomposition of 2-propanol vapour, as a model catalytic reaction, in order to characterize and evaluate the acidity of the tested sulfated aluminas.

Results and Discussions

Characterization of the Catalysts

Crystalline Phases (X-Ray Diffraction, XRD)

Examination of XRD diffractograms, Figs. 1a and 1b, indicates that the impregnation of alumina with sulfate compounds and then calcination at 870 K for 1 h doesn't modify detectably the phase structure of the γ-Al_2O_3. Inspecting the diffractograms and matching with the relevant ASTM standards helps indicating that all sulfate modified catalysts take on the γ-alumina structure (ASTM 29–1486). In fact, the presence of sulfate ions, in such relatively low loading level ($\leq$10%) is not capable of changing the bulk structure of γ-alumina. It seems, however, to act as a crystalline phase stabilizer. It is also acceptable to propose that the sulfate ions are likely to be present as dispersed surface species rather than clusters or multilayers at such relatively low loading. Also, XRD revealed that the introduction of sulfate ions, either from the salt or the acid, onto the *AlO* series (Fig. 1a) renders it slightly more crystalline than the *AlH* series (Fig. 1b), as indicated by the slightly higher XRD peak intensities of the *AlO* series.

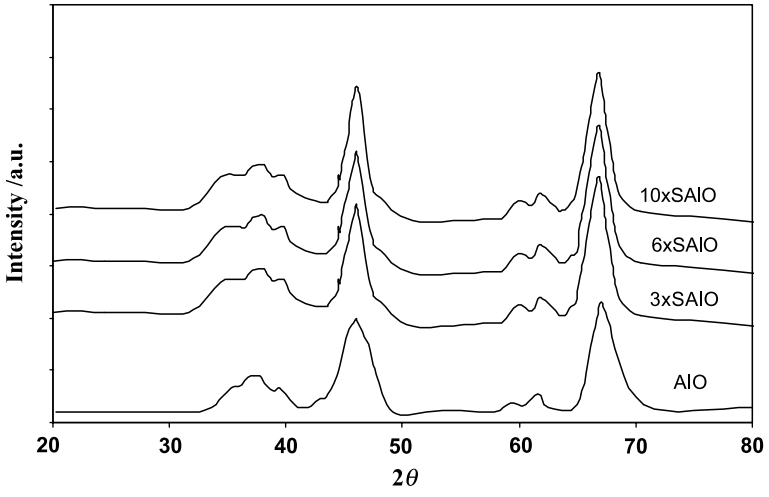

Fig. 1a. X-Ray powder diffractograms of *yxAlO* series of catalysts

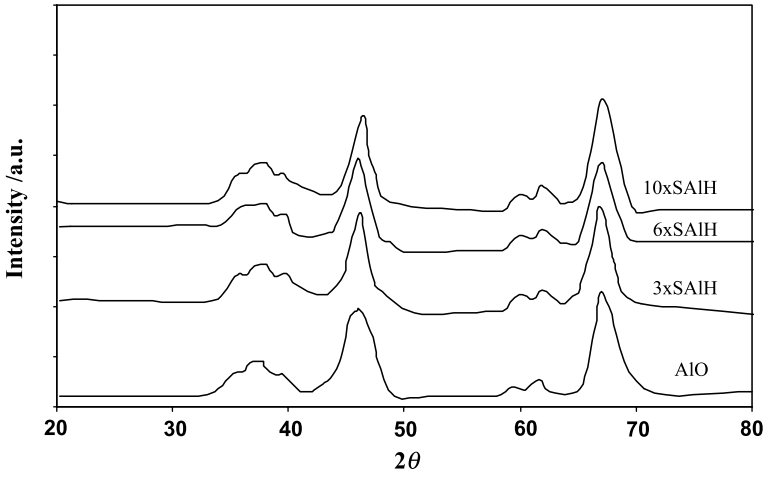

Fig. 1b. X-Ray powder diffractograms of *yxSlH* series of catalysts

Nitrogen Adsorption

The nitrogen adsorption–desorption isotherms at 77 K of sulfate modified aluminas in comparison with pure oxide (γ-Al_2O_3) are illustrated in Figs. 2a and 2b. It can be concluded that all isotherms belong to type IV according to the BET classification [13], and the hysteresis loops are of type H3. Textural data for all the investigated catalysts are compiled in Table 1. The *AlH* series exhibits the higher S_{BET} areas as compared to the *AlO* series. The addition of sulfate, either from the salt or from the acid, onto *AlO* and onto *AlH* results in an S_{BET} decrease as the loading level of sulfate increases from 3 to 10%. This is most likely attributable to elimination of available surfaces either external or (probably internal, noticeable decrease in $V_{p(total)}$ with the increase in sulfate loading for both

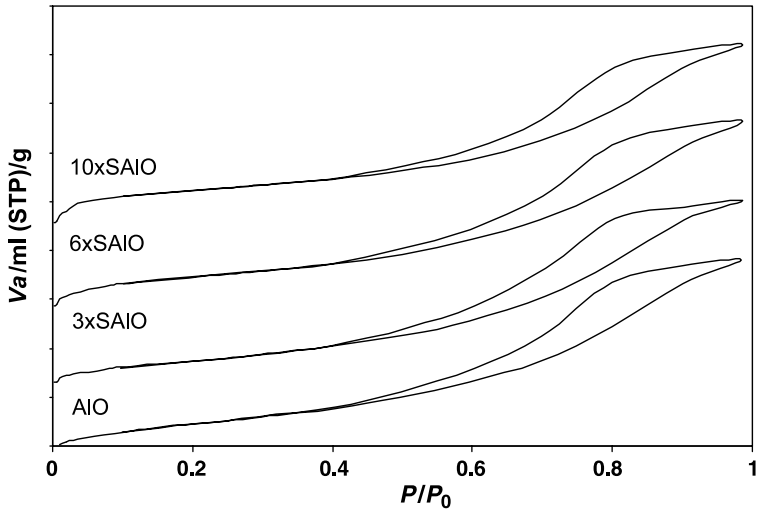

Fig. 2a. N_2 adsorption–desorption isotherms of *yxAlO* series of catalysts

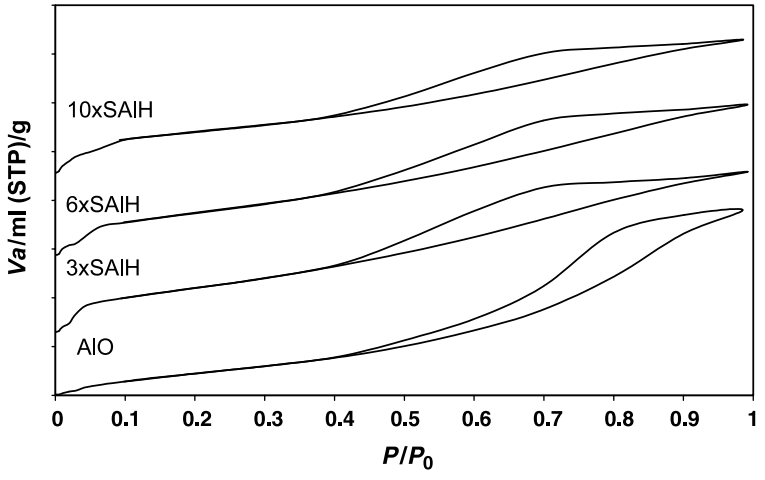

Fig. 2b. N_2 adsorption–desorption isotherms of *yxAlH* series of catalysts

AlO and *AlH* series can be perceived, Table 1) upon sulfation. The differences between S_{BET} and S_{cum} for most catalysts indicate that considerable surfaces are contained in narrow pores. This is also supported by the higher values of $V_{p(total)}$ as compared to $V_{p(cum)}$. Data cited in Table 1 also indicate that the values of $V_{p(cum)}$ decrease with the increase in sulfate content particularly for the 10% loaded catalysts. The modifications observed for the surface texture were further predicted by pore analysis using the t-method [14, 15]. The analysis facilitated detection and differentiation between the micro- and meso-pores for all the sulfated catalysts. The close agreement of S_{BET} and S_t values for most of the catalysts, thereby fulfilling the main criteria [16] for the correct choice of the t-curves used in the analysis.

Table 1. Texture data of alumina and sulfated alumina catalysts

Catalyst	$S_{BET}/m^2 \cdot g^{-1}$	S_t[a]$/m^2 \cdot g^{-1}$	$S_{cum}/m^2 \cdot g^{-1}$	Pore volume/ $cm^3 \cdot g^{-1}$		Particle size[d]/nm
				$V_{p(cum)}$[b]	$V_{p(total)}$[c]	
AlO	187	193	116	0.18	0.34	33
3SAlO	190	198	117	0.18	0.34	35
6SAlO	160	172	103	0.15	0.30	37
10SAlO	130	134	87	0.13	0.26	50
3xSAlO	185	189	111	0.16	0.34	40
6xSAlO	184	176	110	0.15	0.33	41
10xSAlO	179	172	103	0.14	0.31	39
3SAlH	226	220	112	0.18	0.31	31
6SAlH	215	217	111	0.18	0.29	31
10SAlH	187	179	91	0.15	0.24	40
3xSAlH	250	258	116	0.18	0.29	31
6xSAlH	237	240	110	0.18	0.28	31
10xSAlH	210	201	94	0.15	0.24	32

[a] Surface area derived from t-method (Refs. [30–32]); [b] cumulative pore volume (Refs. [30–32]); [c] total pore volume determined at $P/P_0 = 0.99$ (Refs. [30–32]); [d] particle size derived from *Debye* equation (see Ref. [33])

IR Spectroscopy

Hydroxyl Stretching and Sulfate Regions (3900–3300 and 1500–1000 cm^{-1})

The IR results of *AlO* (not shown) indicated the presence of four bands at $\bar{\nu} = 3780$, 3730, 3690, and 3580 cm^{-1}. The first three bands are due to the isolated hydroxyl (OH) groups [17]; whereas the fourth weak broad band at $\bar{\nu} \sim 3580\,cm^{-1}$ is due to hydrogen bonded OH [18]. Types of alumina OH surface groups have been extensively investigated and discussed [18–20] and do not need here any further discussion. The spectrum of *3xSAlO* is found to display bands similar to those found for *AlO*. The other sulfated catalysts (not shown) were found to be largely similar amongst themselves. They were found to display a new band at $\bar{\nu} \sim 3640\,cm^{-1}$ – in addition to the bands found for *AlO* – mostly due to bridged *S–OH* groups [9].

The IR spectra of sulfated alumina catalysts in the sulfate region display bands at 1370 cm^{-1} for the 3% loaded catalysts. Increased sulfate content enhances the intensity of the bands and shifts the characteristic $\bar{\nu}$ vibration of S=O groups towards higher values (6%: $\bar{\nu} \sim 1383$ and 10%: $\bar{\nu} \sim 1388\,cm^{-1}$). These shifts are mostly owing to formation of new sulfate species in the case of such sulfate loads. The bands appearing near $\bar{\nu} = 1100\,cm^{-1}$ are not well resolved, undoubtedly due to overlapping. These results point to exclude bulk-like sulfate species [21].

IR Spectra of Adsorbed Pyridine

The IR spectrum of pyridine (*Py*) adsorption on *AlO* is shown to display five bands at $\bar{\nu} = 1613$, 1596, 1578, 1490, and 1445 cm^{-1}. These bands are assigned

to hydrogen bonded and coordinately bonded *Py*. The band at $\bar{\nu} \sim 1613\,cm^{-1}$ (8a *Py*) is due to *Py* coordinatively bound to *Lewis* acid sites of moderate strength [22]. Some authors [22, 23] assigned such sites to tetrahedral aluminum vacancies; the band at $1596\,cm^{-1}$ is due to *Py* coordinatively bonded to octahedral aluminum *Lewis* acid sites [22]. The other bands $\bar{\nu} = 1579$, 1491, and $1445\,cm^{-1}$ are due to *Py* species coordinated to *Lewis* acid sites. No bands around $1540–1550\,cm^{-1}$ due to *Brønsted* acid sites were observed, this indicates the absence of such sites on the alumina surface. As to the sulfated samples, the IR spectrum of *3xSAlO* is shown to display a similar spectrum to that of pure alumina, a weak shoulder is observed only at $1620\,cm^{-1}$. This band (shoulder) is mostly due to strong *Lewis* acid sites. Thus, such sulfate load (3-wt%) is not capable of generating sites responsible for formation of pyridinium ion species. Increasing the sulfate load (6 and 10-wt%) leads to generation of *Brønsted* acid sites (bands at $\bar{\nu} = 1543$ and $1648\,cm^{-1}$). Moreover, the spectra of *6xSAlO* and *10xSAlO* display a band at $\bar{\nu} \sim 1626\,cm^{-1}$ which is assigned to strong *Lewis* acid sites. *Py* ring modes (8a) vibrations (bands at 1626 and $1596\,cm^{-1}$) indicate the presence of at least two different *Lewis* acid sites differing in acidity strength. The IR spectra of *Py* adsorption on sulfated *AlH series* at room temperature are shown in Fig. 3. The spectra are largely similar to those aforementioned of sulfated *AlO* series. The difference lies only in that; the spectrum of *3xSAlH* displays a weak band at $\bar{\nu} \sim 1543\,cm^{-1}$, which could be actually assigned to *Brønsted* acid sites. The adsorption of *Py* clearly demonstrates that the sulfation of alumina leads to the appearance of two different types of *Lewis* acid sites and also to the generation of *Brønsted* acid sites.

Spectra taken from *Py* adsorption on pure and sulfated *AlH* series (*yxSAlH*) at 520 K were shown to exhibit a gradual weakness in the intensity of the bands characteristic of the room-temperature adsorbed species of *Py*, besides slight shifts towards higher frequencies. The spectrum of pure alumina displays in addition to

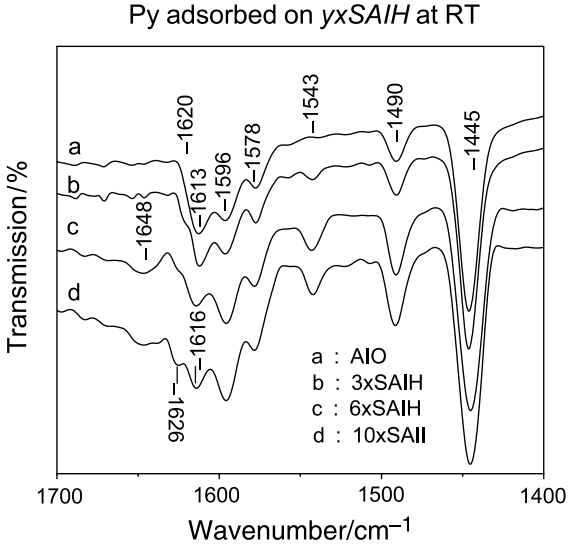

Fig. 3. In situ IR spectra recorded at RT for irreversibly adsorbed *Py* at RT on *yxSAlH* series of catalysts

the bands which appeared at RT, a new band at $\bar{\nu} \sim 1623\,cm^{-1}$. This is most probably due to the presence of strong *Lewis* acid sites, indicating at least two different *Lewis* acid sites. Spectra of *3xSAlH*, *6xSAlH*, and *10xSAlH* display bands characteristic of 8a mode at $\bar{\nu} = 1628$ and $1616\,cm^{-1}$ for *3xSAlH*, 1632 and $1620\,cm^{-1}$ for *6xSAlH*, and 1633 and $1621\,cm^{-1}$ for *10xSAlH*. These bands are generally assigned to *Py* coordinatively bound to strong *Lewis* acid sites, at least more than two different *Lewis* acid sites are present (due most likely to different degrees of coordination unsaturation of Al-cations) [23, 24]. The spectra of sulphated alumina *yxSAlO* samples at 520 K (not shown) are quite similar to those obtained for *yxSAlH* samples.

These results indicate that the presence of SO_4^{2-} species >3-wt% generates *Brønsted* acid sites and at least two different (in acidic strength) types of *Lewis* acid sites. Accordingly, *Lewis* acid sites exposed on sulfated samples are stronger than those exposed on pure alumina. The presence of strong *Lewis* acid sites on the surface of sulfated samples is due to the sulfate groups, which are assumed to withdraw electrons from the metal ion thus enhancing the ability of Al^{3+} ion sites to interact directly with *Py* [25]. On the other hand, *Brønsted* acid sites may be generated by the interaction of *Lewis* acid sites with water molecules.

Catalytic Activity towards 2-Propanol Decomposition

Preliminary experiments for temperature scanning showed that the decomposition of 2-propanol (*2-Pr*OH) on metal oxide catalysts proceeds through simultaneous dehydration and dehydrogenation reactions (at $\geq$520 K as reaction temperature). *2-Pr*OH dehydrates at 520 K producing propene. Therefore, the results of *2-Pr*OH decomposition at 520 K on test catalysts are listed in Table 2. Since the alumina surface is dominated by acid sites (*Py* adsorption), it is clear that it exhibits higher

Table 2. 2-Propanol and its decomposition products on alumina and sulfated alumina catalysts at 520 K

Catalyst	Conversion/% Isopropanol	Percentage selectivity	
		Propene/%	Acetone/%
AlO	79.2	94.2	5.8
3SAlO	89.1	95.3	4.7
6SAlO	100.0	97.6	2.4
10SAlO	97.3	96.5	3.5
3xSAlO	92.0	95.5	4.5
6xSAlO	100.0	97.9	2.1
10xSAlO	97.5	96.7	3.3
3SAlH	90.7	95.4	4.6
6SAlH	100.0	98.2	1.8
10SAlH	97.6	96.8	3.2
3xSAlH	92.2	95.8	4.2
6xSAlH	100.0	98.4	1.6
10xSAlH	97.9	97.0	3.0

dehydration (propene) selectivity 94.2%, Table 2. All sulfated catalysts exhibit higher decomposition activity than pure alumina. Also, the propene selectivities are slightly higher than on pure alumina. The results cited in Table 2 also indicate that the decomposition of *2-Pr*OH increases with increasing the sulfate loading level from 3 to 6-wt%. The 6-wt% loaded catalysts show the highest (100%) decomposition activity and the highest propene selectivity. These results are in fair agreement with the results observed by *Waqif et al*. [26] for the conversion of methanol on sulfated alumina.

The high *2-Pr*OH dehydration on alumina is due to the presence of strong surface *Lewis* acid sites [26]. Hence, the increase in the dehydration activity of the sulfated catalysts can be related to the increase of the acidity of *Brønsted* acid sites and/or to the increase of the number of *Lewis* acid sites. This seems to be a maximum for the 6-wt% loaded catalysts, this series also is shown to withstand losses in surface area and pore volume better than the 10-wt% loaded catalysts (Table 1). Hence better dispersion and exposure of active sites can be expected for the 6-wt% loaded catalysts.

Experimental

Materials

Pure alumina, denoted in the text as *AlO*, was obtained from alumina gel by calcination at 870 K for 3 h. The gel denoted in the text as *AlH*, was prepared according to *Lippens* [27] by a dropwise addition of a (1:1) solution of NH_4OH (AR-grade, Prolabo product) to a 0.1 *M* solution of $Al(NO_3)_3 \cdot 9H_2O$ (AR-grade, BDH product).

Two series of sulfated alumina catalysts were obtained by impregnation of *AlO* and *AlH* with an aqueous solution of $(NH_4)_2SO_4$ or H_2SO_4; which has been held stirred for 1 h. The impregnating solutions were adjusted to give 3, 6, and 10-wt% SO_4^{2-} content. The catalysts were obtained by calcination of the dried samples at 870 K for 1 h. The amount loaded (6-wt%) was calculated to be similar to that needed to cover the entire support surface in the case of a homogenous dispersion (area of $SO_4^{2-} = 25$ Å^2) [28]. Two other sulfate loads were taken; a lower one with 3-wt% and a higher one with 10-wt% SO_4^{2-}. For convenience, the calcination products obtained are designated in the text as *ySAlO*, *yxSAlO, ySAlH*, and *yxSAlH*; where *y* is the loading level and *x* signifies that the impregnating sulfate solution is H_2SO_4.

Catalyst Characterization Methods and Techniques

X-Ray Diffraction (XRD)

XRD diffractograms were recorded for all samples using a model JSX-60PA JEOL diffractometer (Japan) equipped with a source of Ni-filtered, CuK_α radiation ($\lambda = 1.5418$ Å). The generator was operated at 35 kV and 20 mA. For identification purposes, diffraction patterns (I/I^o) *versus d* spacing (Å) were matched with the relevant ASTM standards [29].

Nitrogen Adsorption

Full nitrogen adsorption/desorption isotherms at −196°C were obtained using a NOVA 2000, version 6.10 high-speed gas sorption analyzer (Quantachrome Corporation USA). The calcined samples were first outgassed at 470 K for 1 h prior to adsorption measurements. Various specific surface areas (S_{BET}, S_{cum}, and S_t) were determined by adopting appropriate methods [30, 31] for the analysis of the N_2-adsorption isotherms. Surface texture, surface area analysis, and porosity estimations were performed using standard and well-established methods.

Infrared Spectroscopy

IR spectra were obtained at a resolution of $4\,cm^{-1}$, in the range of 4000–500 cm^{-1}, using a Genisis-II FT-IR spectrophotometer, Mathson (USA). For pyridine (*Py*) adsorption on test samples, a wafer of 15–20 mg/cm^2 was mounted in a Pyrex vacuum cell fitted with CaF_2 windows. The samples were pretreated at 700 K for 1 h in a stream of O_2 followed by evacuation at 700 K for 1 h, then cooled to room temperature to obtain the background IR spectra. Then, 5 Torr *Py* (1 Torr = 133.32 Pa) were admitted at various temperatures (300–570 K) for 5 min, degassed for 5 min at each temperature in order to remove physisorbed *Py*, and the spectra were then taken at room temperature.

Catalytic Activity (2-Propanol Decomposition)

The catalytic activity experiments for 2-propanol (*2-Pr*OH) decomposition were carried out in a fluidized bed quartz flow reactor at atmospheric pressure. Portions of 0.2 g of the catalyst were activated in-situ at 670 K for 1 h in N_2. *2-Pr*OH (Merck, 99.9%) was introduced at a flow rate of $14.8\,cm^3 \cdot min^{-1}$ into the carrier gas flow of N_2. The reaction products were analyzed by gas chromatography on a 2 m long $1/8''$ column packed with 10% Carbowax and Chrom WHP 80/100 using a model 3400 Varian Gas Chromatograph equipped with a flame ionization detector (FID).

Acknowledgements

We acknowledge with appreciation the GC equipment donation (V-8151/87039; c/o Prof. *Mohamed I. Zaki* of Minia University) by the *Alexander-von-Humboldt-Foundation*, Bonn/Germany.

References

[1] Gates BC (1992) Catalytic Chemistry. Wiley, New York
[2] Thomas JM, Thomas WJ (1996) Principles and Practice of Heterogeneous Catalyst. VCH, New York
[3] Ertel G, Knözinger H, Weitkamp J (1997) Handbook of Heterogeneous Catalysis. Wiley-VCH, New York
[4] Clearfield A, Serrette GPD, Khazi-Syed AH (1994) Catal Tod **20**: 295
[5] Morterra C, Cerrato G, Pinna F, Signoretto M (1995) J Catal **157**: 109
[6] Norman CJ, Gaulding PA, McAlpine I (1994) Catal Tod **20**: 313
[7] Arata K (1990) Adv Catal **37**: 165
[8] Spielbauer D, Mekhemer GAH, Zaki MI, Knözinger H (1996) Catal Lett **36**: 59
[9] Riemer T, Spielbauer D, Hunger M, Mekhemer GAH, Knözinger H (1994) J Chem Soc Chem Comm 1181
[10] Yamaguchi T, Jin T, Tanabe K (1986) J Phys Chem **90**: 3148
[11] Yamaguchi T (1990) Appl Catal **61**: 1
[12] Alexander FB, Kenneth JK (1998) J Catal **176**: 448
[13] Brunauer S, Emmett PH, Teller T (1938) J Am Chem Soc **60**: 309
[14] Lippens BC, Linsen BG, De Boer JH (1964) J Catal **3**: 32
[15] De Boer JH, Linsen BG, Osinge J (1965) J Catal **4**: 643
[16] Mikhail RSh, Sheb F (1970) J Colloid Interf Sci **34**: 65
[17] Beri JB, Hannan RB (1960) J Phys Chem **64**: 1526
[18] Ballinge TH, Yates T Jr (1991) Langmuir **7**: 3041
[19] Peri JB (1965) J Phys Chem **69**: 220
[20] Knözinger H, Ratnasamy P (1978) Catal Rev Sci Eng **17**: 31
[21] Bensitel M, Waqif M, Saur O, Lavalley JC (1989) J Phys Chem **93**: 6581
[22] Morterra A, Chiorino A, Ghiotti G, Garrone E (1979) J Chem Soc Farady Trans I **75**: 271
[23] Morterra C, Coluccia S, Chiorino A, Boccuzzi F (1978) J Catal **54**: 348

[24] Zaki MI, Hussein GAM, Mansour SAA, El-Ammawy HA (1989) J Mol Catal **51**: 209
[25] Jin T, Yamaguchi T, Tanabe K (1986) J Phys Chem **90**: 4794
[26] Waqif M, Baachelier J, Saur O, Lavalley JC (1992) J Mol Catal **72**: 127
[27] Lippens BC (1961) PhD Thesis. Delft University, The Netherlands
[28] Bedilo AE, Kim VI, Volodin AM (1998) J Catal **176**: 294
[29] Smith JV (Edn) (1960) X-ray Powder Data File. American Soc for Testing and Materials, Philadelphia, PA
[30] Gregg SJ, Sing KSW (1982) Adsorption, Suface Area and Poosity, 2nd edn. Academic Press, London
[31] Lecloux A (1981) In: Anderson JR, Boudart M (eds) Catal-Sci & Techn, Springer, Berlin
[32] Nohman AKH, Mekhemer GAH, Fouad NE, Khalaf HA (1999) Adsorption Sci Technol **17**: 8
[33] Debye P (1915) Ann Phys **46**: 809